Expression of transduced Nucleolin promotes the clearance of accumulated alpha-synuclein

DONG HWAN HO (ethan2887@gmail.com)
Wonkwang University https://orcid.org/0000-0003-4938-4108
Daleum Nam
Wonkwang University
Soyeon Jeong
Wonkwang University
Mi Kyoung Seo
Inje University
Sung Woo Park
Inje University
Wongi Seol
Wonkwang University
Ilhong Son
Wonkwang University

Research article

Keywords: Parkinson's disease, α-synuclein, nucleolin, gene therapy

Posted Date: July 14th, 2020

DOI: https://doi.org/10.21203/rs.3.rs-39766/v1

Abstract

Background

Alpha-synuclein (αSyn) is a major component of Lewy bodies, which are known to be a pathogenic marker of Parkinson's disease (PD). The accumulation of αSyn is caused by dysfunctions in protein degradation machinery. The reinforcement of αSyn degradation is a potential therapeutic target of PD since accumulated αSyn is responsible for the pathogenesis of PD. Nucleolin (NCL) is essential for forming nucleolar structure. The function of NCL is correlated with oxidative stress-mediated cell death. A previous study demonstrated that NCL was reduced in PD brains, and overexpression of NCL alleviated rotenone-induced neural toxic effects. Knockdown of NCL had the opposite effect. These results suggest that the malfunctioning of NCL would exacerbate PD pathology. Thus, we hypothesized that the introduction of ectopic NCL could rescue the α-synucleinopathy in PD.

Methods

We tested whether ectopic expression of NCL facilitates the clearance of αSyn. The Ectopic expression of NCL was accomplished by the transfection of GFP or GFP-NCL in mouse embryonic fibroblasts (MEF) or transduction of green fluorescent protein (GFP) or GFP-NCL using lentivirus in rat primary cortical neuron. We also investigated whether the expression of GFP or GFP-NCL in mouse substantia nigra alleviates the PD pathology derived by αSyn aggregates.

Results

The expression of NCL enhanced the clearance of αSyn accumulation or aggregates in MEF and rat primary cortical neurons. The activity of autophagy-lysosome pathway was enhanced by NCL expression. The transduction of NCL in the substantia nigra, which was co-injected with αSyn fibrils, rescued PD manifestations.

Conclusions

The elevation of NCL levels may reflect a therapeutic strategy for α-synucleinopathy in PD.

Background

Parkinson's disease (PD) is the second most common neurodegenerative disease. A loss of dopaminergic neurons in the substantia nigra pars compacta (SNpc) is a primary cause of PD pathogenesis (1). The protein inclusion composed by alpha-synuclein (αSyn) in a surviving neuron is referred to as a Lewy body (LB) or Lewy neurite (LN), and LBs/LNs are a pathologic marker for the postmortem study of PD (2). The αSyn aggregates are generated by defective clearance of misfolded αSyn (3). In a spatiotemporal

manner, the accumulation of misfolded αSyn that underwent a conformation change from random coils to beta sheets accelerates the aggregation of αSyn in the neuron (4). In previous reports, the propagation of αSyn aggregates throughout the brain was revealed to be a critical pathomechanism of PD along with aging (5–7). The blockage or clearance of αSyn aggregates is currently being investigated as a drug target of PD therapy (8, 9).

Nucleolin (NCL) is one of the components for maintaining a nucleolar structure (10). NCL involves several cellular mechanisms, such as damaged DNA repair and protein degradation, because NCL function is strongly linked with the survival of cell death (11–14). Anti-apoptotic molecule heat shock protein 70 (HSP70) was reported to be a regulator of NCL fate (15). In a previous study, PD patients showed a reduction in NCL levels from the lysate of the SNpc compared to control patients. In addition, NCL overexpression ameliorated oxidative stress cytotoxicity initiated by the treatment of rotenone, a PD-inducing drug, while the silencing of NCL expression aggravated rotenone-induced reactive oxygen species (ROS) and cell death (16).

Since cellular ROS can be crucial for the accumulation and aggregation of αSyn in dopaminergic neurons (17), we hypothesized that the introduction of NCL would also play a role in the clearance of αSyn aggregates, thereby mitigating α-synucleinopathy. Our research herein elucidated that the ectopic expression of NCL in mouse embryonic cells and the mouse SNpc alleviates the accumulation of αSyn and degrades αSyn via the autophagy-lysosome pathway.

Methods

Cell culture, transfection, harvest, and immunostaining

We cultured mouse embryonic fibroblasts (MEFs) with high glucose Dulbecco's Modified Eagle Medium (DMEM, 10-013-CV; Corning Cellgro, Manassas, VA, USA), 10% fetal bovine serum (FBS, 35-010-CV, Corning Cellgro), and 1% penicillin/streptomycin (P/S,10378-016, Gibco, Grand Island, NY, USA) at 37 ℃ in a 5% CO_2 incubator (Thermo Fisher Scientific, Waltham, MA, USA). We excluded the MEFs over 7 passages because the cells around 10 passages showed senescence-like symptoms. Next, 0.5 μg of Flag-tagged αSyn (Flag-αSyn) with 0.15 μg green fluorescent protein (GFP) or 1.0 μg GFP-NCL plasmid was co-transfected into the MEFs by LipoD293 (SL100668; SignaGen, Rockville, MD, USA) for 24 h. For the sequential transfection using LipoD293, the same amount of GFP or GFP-NCL was transfected for 24 h following 1 μg of Flag-αSyn transfection for 12 h. At the end point of transfection, the cells were harvested with lysis buffer (phosphate-buffered saline [PBS] with 1% Triton X-100 [T8655; United States Biological, Salem, MA, USA] and 1X Xpert protease inhibitor cocktail [P3100; GenDEPOT, Katy, TX, USA]) or fixed with 4% paraformaldehyde (PFA) and stained using Hoechst 33342 (62249; Thermo Fisher Scientific) with following antibodies: anti-DYKDDDK (Flag) tag mouse monoclonal (8146S; Cell Signaling Technology [CST], Danvers, MA, USA) and anti-C23 (NCL) rabbit polyclonal (sc-13057; Santa Cruz Biotechnology, Dallas, TX, USA). The rest of the immunostaining process followed our previous study. For

the staining of LysoTracker™ Red DND-99 (L7528; Invitrogen, Carlsbad, CA, USA) and LysoSensor™ Blue DND-167 (L7533; Invitrogen), we utilized each manufacturer's guide.

Western blot analysis

The samples in lysis buffer were mixed with 5X sample buffer (250 mM Tris-HCl, pH 6.8, 10% sodium dodecyl sulfate, 50% glycerol, 5% β-mercaptoethanol, and 0.1% bromophenol blue). To detect the proteins of interest, we used the following antibodies: anti-DYKDDDK (Flag) tag mouse monoclonal (8146S; CST), anti-DYKDDDK (Flag) tag rabbit polyclonal (2368S; CST), anti-C23 (NCL) rabbit polyclonal (sc-13057; Santa Cruz Biotechnology), anti-Lamin B goat polyclonal (sc-6217; Santa Cruz Biotechnology), anti-HSP90 mouse monoclonal (610418; BD Biosciences, Franklin Lakes, NJ, USA), anti-β-actin mouse monoclonal (sc-47778; Santa Cruz Biotechnology), anti-LC3B rabbit polyclonal (2775S; CST), anti-α-tubulin mouse monoclonal (T5168; Sigma-Aldrich, St. Louis, MO, USA), anti-GFP rabbit poly clonal (ab290; Abcam, Cambridge, UK), and anti-α-synuclein (clone 42) mouse monoclonal (610786; BD Biosciences). We performed the western blot analysis as described in our previous study (18). Images of the nitrocellulose membrane were captured with a MicroChemi 4.2 camera (Shimadzu, Kyoto, Japan).

Isolation of mRNA and synthesis of cDNA

We performed mRNA isolation using a RNeasy Plus Kit (QIAGEN, Hilden, Germany), and we used a SuperScript™ III First-Strand Synthesis Kit (11752050; Invitrogen) for the cDNA synthesis. To amplify cDNA and detect target DNAs, we used the following primers: Flag tag forward: TAC AAG GAT GAC GAT GAC AAG CTT, Flag-αSyn reverse: GGC TTC AGG TTC GTA GTC TTG, CTSD forward: TGT TAC CAA CTG GGA CGA CA, CTSD reverse: TCT CAG CTG TGG TGG TGA AG, LAMP1 forward: ATG GCC AGC TTC TCT GCC TCC, LAMP1 reverse: ATG GCC AGC TTC TCT GCC TCC, LC3B forward: AGC AGC ACC CCA CCA AGA TC, LC3B reverse: GTG CCC ATT CAC CAG GAG GAA G, β-actin forward: TGT TAC CAA CTG GGA CGA C, and β-actin reverse: TCT CAG CTG TGG TGG TGA AG. After polymerase chain reaction (PCR), the samples were mixed with LoadingSTAR dye (Dyne Bio Inc., Seongnam, South Korea), and the mixed PCR products were subjected to 2% agarose gel made of HiQ Standard Agarose (GenDEPOT). Images of the agarose gel were captured by G: BOX (Syngene, Bangalore, India).

Cathepsin D activity assay

The cells were harvested with the lysis buffer offered by the manufacturer of the Cathepsin D Activity Fluorometric Assay Kit (#K143-100; Biovision Inc., Milpitas, CA, USA). The lysed mouse midbrains were mixed with the lysis buffer in the kit to make a 3 mg/mL protein concentration. Then, we followed the manufacturer's guidance for the measurement of Cathepsin D activity.

Uptake of αSyn fibrils

The generation of αSyn fibrils was described in our previous report (19). We transfected cells with 0.15 μg GFP or 1.0 μg GFP-NCL using LipoD293 for 24 h following the 6 h pre-treatment of 700 nM αSyn fibrils. We harvested the cells with lysis buffer or fixed them with 4% PFA and used an Aggresome staining kit (Enzo Life Sciences, Farmingdale, NY, USA) according to the manufacturer's instructions.

Enzyme-linked immunosorbent assay (ELISA) for αSyn

In our previous study, we performed a sandwich ELISA and measured the amount of total αSyn by anti-α-synuclein [clone #42] (610787; BD Biosciences) or fibrillar αSyn oligomer by anti-α-synuclein filament antibody [MJFR-14-6-4-2] (ab209538; Abcam) in both the culture media and cell lysates (20). The culture media containing αSyn fibrils and the lysed mouse midbrain (0.1 mg/mL) was subjected to our established ELISA kit.

Lentivirus production

Two types of lentivirus, Lenti-GFP and Lenti-GFP-NCL, have been produced. The Lenti-GFP viral vectors were obtained from CdmoGen (Cheongju, South Korea) and used to clone the full length human nucleolin gene. The sequence of nucleolin in the resulting Lenti-GFP-NCL vector was confirmed. Both purified Lenti-GFP and Lenti-GFP-NCL plasmids were used to produce lentiviral vectors by CdmoGen, and their titers were $1.51 \cdot 10^{10}$ and $3.39 \cdot 10^{10}$ copies/mL, respectively.

Preparation of rat primary cortical neurons

The isolation and culture of rat primary cortical neurons were described in the previous report (21). The lentiviruses of GFP or GFP-NCL were transduced with 40 MOI in the rat primary cortical neurons ($4 \cdot 10^8$) for 4 8 h following the treatment of αSyn fibrils for 24 h. The cells were harvested with 1X sample buffer (50 mM Tris-HCl, pH 6.8, 2% sodium dodecyl sulfate, 10% glycerol, 1% β-mercaptoethanol, and 0.02% bromophenol blue) before we proceeded with western blot analysis. The culture media was collected and subjected to ELISA.

Mouse handling and stereotaxic injection

After receiving the 15-week-old C57BL/6J mice (Daehan Biolink, Samseong, South Korea), we left them to stabilize for approximately 1 week in the animal room. The animal room was designed with a 12-hour day and night cycle in an environment limited to an internal temperature of 23 ± 2 °C, internal humidity of 55 ± 5%, and illuminance of 300 Lux. Food (Daehan Biolink) and water were provided at random, and all processes for breeding and management were conducted in accordance with the provisions of the Dankook Animal Ethics Committee (Dankook IACUC, 18–026). Animals anesthetized during stereotaxic surgery were recovered using a heating pad, and experiments that required training before being performed were repeatedly practiced in advance to manage any feelings of heterogeneity in the behavioral test equipment.

The lentiviruses of GFP ($1.5 \cdot 10^7$ pfu) or GFP-NCL ($3 \cdot 10^7$ pfu) mixed with 500 ng of αSyn fibrils (dissolved in PBS) were microinjected into the SN of nine 16-week-old C57BL/6J male mice. The microinjection was performed with a stereotaxic apparatus (Kopf instrument), and the injection cannula was inserted by accessing AP -3.0 mm, ML + 1.2 mm, and DV -4.5 mm from the bregma. The flow rate of injection was 0.25 μL/min for 4 min, and we waited for an additional 5 min to allow the drug to be

completely absorbed. For each animal, 1 uL of treatment was microinjected. Subjects were examined using the rotarod test at 3 and 6 weeks after injection.

Mouse brains were dissected to obtain the midbrain. Midbrain tissues were lysed with the lysis buffer containing 1X phosphatase inhibitor cocktail using a Pellet Pestle Cordless Motor (Sigma-Aldrich). We centrifuged the crude extracts of the midbrain at 400 · g at 4 ℃ for 30 min following 30 min of incubation on ice. Then, the supernatants were subjected to western blot analysis, a Cathepsin D activity assay, and ELISA.

Rotarod test

The mice were examined on a rotatable cylinder-shaped rod about 3 cm in diameter, and the speed of the rota-rod was accelerated slowly from 4 rpm to 40 rpm. We recorded the time that it took for each mouse to fall to the floor, and the object that maintained the motion without falling until 10 min stops the rod and recorded it as 600 s. The test was repeated 3 times per subject, and the subjects were allowed to rest for at least 15 min intervals between each test.

Immunohistochemistry

The perfused brains were sectioned at 20 μm thickness, and immunohistochemistry was performed as described previously (22). Briefly, free-floating sections were washed in 0.1 M PBS, quenched with 1% H_2O_2, and incubated at 48 °C with the primary antibodies anti-tyrosine hydroxylase (1:500, ab112; Abcam) and anti-phospho-α-synuclein (1:500, 015-25191; Wako Chemicals, Osaka, Japan) comprised of 1% bovine serum albumin, and 0.3% TritionX-100 in PBS. Incubation with the appropriate biotinylated secondary antibodies (1:250) was followed by incubation in avidin-biotin-peroxidase solution (VECTASTAIN Elite ABC Kit; Vector Laboratories, Burlingame, CA, USA). The reaction was visualized using 3'-diaminobenzidine (DAB), dehydrated in ethanol, cleared in xylene, and coverslipped with DPX Mounting Medium (Sigma-Aldrich).

Immunofluorescent staining

Brain sections were blocked with 10% bovine serum albumin in PBS containing 0.2% Triton X-100 and then immunostained with microglial marker anti-rabbit Iba1 antibody (1:400, 010-19741; Wako Chemical) in blocking solution at 4 °C overnight. The sections were then incubated at room temperature for 1 h with goat anti-rabbit IgG-488 antibody (1:200; Life Technologies, Carlsbad, CA, USA), counterstained with DAPI (4',6-diamidino-2-phenylindole, 1:2000; Roche Life Science, Branford, CT, USA), and mounted using DAKO Fluorescent Mounting Medium (S3023; Agilent, Santa Clara, CA, USA).

Image analysis

Pictures of the sections were taken using an Olympus BX 51 microscope (Tokyo, Japan). The National Institutes of Health (NIH) image program (ImageJ; Bethesda, MD, USA) was used to determine optical densities (ODs) and cell count.

Data analysis

The densitometers of the protein bands of interest were measured using the Gauge V 3.0 program (Fujifilm, Tokyo, Japan). Intensities of the stained protein were estimated with ZEN (ZEISS, Oberkochen, Germany). The puncta numbers of LysoTracker, LysoSensor, and Aggresome were counted by ImageJ (NIH) in GFP-positive cells. All data sets were analyzed and diagrammed with Prism 8 (GraphPad Software, San Diego, CA, USA). In each figure legend, we describe the respective statistical analyses.

Results

1. Overexpression of αSyn disrupts the recruitment of NCL in the nucleolus

In a previous study, the SNpc lysate from PD patients showed a decrease in NCL levels compared to control patients, and rotenone treatment in a dopaminergic neuron cell line (MES) reduced the levels of NCL in a time-dependent manner (16). The increase in αSyn by rotenone treatment and αSyn aggregates in the SNpc of PD are reported to be a pathological mechanism for PD. To test whether the overexpression of αSyn affects NCL levels, we transfected Flag-αSyn into MEF cells for 24 h. Nuclear endogenous NCL (endoNCL) levels were significantly decreased in the transfected Flag-αSyn cells compared to the control vector-transfected cells. (Fig. 1A). Cellular expression of Flag-αSyn decreased the number of nucleolar puncta (Supplementary Fig. 1). The interaction of NCL with αSyn in the cytosol was demonstrated in a previous study (23). In addition, the localization of αSyn was studied to determine a distinct cause of the pathogenesis of PD. Thus, we synthesized a nuclear localization signal (NLS) or nuclear escape signal (NES) on Flag-αSyn, and we transfected those genes into MEFs. Immunofluorescence analysis revealed that the intensity of endoNCL in the nuclei was decreased in transfected wild type Flag-αSyn (WT-αSyn) and NES Flag-αSyn (NES-αSyn) cells relative to transfection gene empty cells (Empty). Meanwhile, NLS Flag-αSyn expression (NLS-αSyn) showed a significant increase in nuclear endoNCL levels compared to WT or NES Flag-αSyn but similar to Empty (Fig. 1B). In line with a previous report (24, 25), we observed that expression of NLS-αSyn exhibited higher cytotoxicity than WT- or NES-αSyn (Supplementary Fig. 2). We assumed that nuclear αSyn might play a distinct toxicity role in PD and concluded that αSyn accumulation and aggregation would be related to a decrease in NCL levels.

2. Elevated αSyn is degraded by the ectopic expression of NCL

Ectopic expression of NCL ameliorated the rotenone-induced neurite shortening and cytotoxicity in a previous study (16). These symptoms are associated with αSyn-derived neuronal death (26). To clarify the therapeutic effects of NCL, we co-transfected Flag-αSyn with GFP or GFP-NCL into MEFs. The expression of GFP-NCL significantly decreased the levels of Flag-αSyn in TritonX-100 soluble (Tx-100 sol) and TritonX-100 insoluble (Tx-100 insol) fractions (Fig. 2A). The degradation of Flag-αSyn in Tx100 insol was demonstrated in similar experiments with the human embryonic kidney cell line HEK-293T (Supplementary Fig. 3A).

To utilize NCL as a therapeutic target for PD caused by the accumulation of αSyn, it is necessary to sufficiently express αSyn in the cells before the expression of NCL, thereby proving the therapeutic effect while excluding the possibility of NCL-mediated αSyn gene expression. For the confirmation of NCL-mediated αSyn clearance in MEF cells, we transfected GFP or GFP-NCL for 24 h following Flag-αSyn transfection for 12 h. We observed that the transfection of GFP-NCL significantly decreased the levels of Flag-αSyn in Tx100 insol along with the induction of LC3B II/I levels (Fig. 2B). However, the short expression (12 h) of GFP-NCL showed no significant change in the levels of Flag-αSyn (Supplementary Fig. 3B). To demonstrate that expression of NCL does not cause a reduction in all transduced genes, we tested Flag-tagged p21 (Flag-p21) instead of Flag-αSyn. The ectopic expression of NCL did not reduce the levels of Flag-p21 in both Tx100 sol and insol (Supplementary Fig. 4). To verify that the decrease in Flag-αSyn does not relate to transcriptional changes, we measured the mRNA levels of Flag-αSyn. There were no differences in Flag-αSyn mRNA levels between the expression of GFP and GFP-NCL (Supplementary Fig. 5). Taken together, introduction of NCL could promote the clearance of accumulated αSyn.

3. NCL-mediated clearance of αSyn is accomplished via the autophagy-lysosome pathway

The accumulated αSyn is mainly degraded via the autophagy-lysosome pathway (27). Because the ectopic expression of NCL showed an increase in the cleavage of LC3B II form LC3B I in Tx-100 insol, which represents the induction of autophagosome formation (Fig. 2B), we next investigated the αSyn degradation pathway by expression of NCL. The expression of GFP-NCL showed significant increases in the mRNA levels of the autophagy-lysosome pathway, including Light Chain 3B (LC3B), lysosome-associate membrane protein 1 (LAMP1), and cathepsin D (CTSD) (Fig. 3A). The enzymatic activity of CTSD, which is known as a crucial lysosomal enzyme for the degradation of αSyn, was increased in the transfection of GFP-NCL relative to GFP controls (Fig. 3B). The comparison of lysosome numbers in a single MEF cell using LysoTracker demonstrated that GFP-NCL-expressing cells exhibited higher lysosome numbers (7.8 ± 0.2) than the GFP controls (10.7 ± 0.2; Fig. 3C). Moreover, we used LysoSensor to detect the active lysosome, which is acidic. The numbers of LysoSensor puncta in GFP-NCL-expressing MEFs (4.2 ± 2.4) showed a significant increase compared to the GFP controls (1.7 ± 0.2; Fig. 3D). To confirm the degradation of αSyn via the autophagy-lysosome pathway, we tested several proteolytic inhibitors, including 3- Methyladenine (3-MA), MG132, Bailomycin A1 (Baf A1), and NH_4Cl. The inhibition of the autophagosome using 3-MA abolished the effect of GFP-NCL on the clearance of Flag-αSyn in both fractions of Tx-100 sol and insol. However, MG132, a proteasome inhibitor, did not affected the degradation of Flag-αSyn (Figs. 4A and 4B). In the fraction of Tx-100 sol, the inhibitor of autophagy-lysosome fusion, Baf A1, promoted a slight increase in Flag-αSyn levels compared to GFP-NCL (Fig. 4C). Treatment with NH_4Cl, which neutralizes lysosomal pH, did not alter the levels of Flag-αSyn (Fig. 4C). However, treatments with BafA1 or NH_4Cl diminished the effect of GFP-NCL expression on the degradation of Flag-αSyn in the fraction of Tx-100 insol (Fig. 4D). MG132 treatment did not affect GFP-NCL-mediated Flag-αSyn degradation in both Tx-100 sol and insol fractions (Fig. 4). These results suggest that the autophagy-lysosome pathway would be a major mechanism of Flag-αSyn degradation.

4. αSyn Fibrils Are Degraded By Ectopic Ncl Expression

Fibrillar formation of αSyn is the predominant form of the accumulated and aggregated αSyn in dopaminergic neurons (28). As shown in Fig. 5A, the uptake of recombinant αSyn fibrils (Fibril) significantly reduced the levels of NCL compared to vehicle treatment (PBS) but only slightly relative to treatment with monomer recombinant αSyn (Mono). Next, we validated the effect of NCL overexpression on αSyn degradation using Fibril. The overexpression of GFP-NCL accelerated the degradation of Fibril in Tx-100 insol via the induction of LC3BI and its cleavage to LC3B II (Fig. 5B). On the other hand, silencing of NCL did not alter Fibril degradation or autophagy-lysosomal markers, such as LC3B and CTSD (Supplementary Fig. 6). In order to visualize the clearance of αSyn aggregates in MEFs, the internalized αSyn fibrils were analyzed using an Aggresome detection kit. We observed that signal of the Aggresome detection kit was colocalized with the signals from the αSyn antibody in MEFs (Supplementary Fig. 7A). The intensity of aggregates was not changed by the expression of GFP-NCL, but the number of aggregate puncta along with the distribution of their size was significantly decreased in GFP-NCL-transfected MEFs (Fig. 5C). Furthermore, the massive inclusions (> 6 μm^2) were only observed in GFP-expressing MEFs (arrowheads in Fig. 5C). Because the expression of GFP or GFP-NCL could disrupt the Fibril uptake efficiency in MEFs, we tested endocytosis rates using Qtracker 655 dye. There was a slight increase in Qtracker uptake in the expression of GFP-NCL compared to the GFP controls (Supplementary Fig. 7B). We performed a sandwich ELISA for total amount of αSyn (Total-αS) or MJFR-14-6-4-2 antibody-specific fibril αSyn (Fila-αS) (20). Both ELISA analyses revealed that the amount of Total- and Fila-αS remaining in the culture media was significantly decreased by the expression of GFP-NCL (Figs. 5D and 5E). These results support the positive effect of NCL introduction on the degradation of αSyn aggregates and suggest that extracellular αSyn aggregates may be also cleared by the expression of NCL.

5. Transduction of NCL in primary neurons enhanced the degradation of internalized αSyn aggregates

To elucidate the association of αSyn aggregates with NCL in neurons, we applied αSyn fibrils onto mouse primary cortical neurons. Fibril treatment significantly decreased the levels of endoNCL relative to PBS controls (Fig. 6A). Next, the degradation of αSyn via the transduction of NCL was verified using mouse primary cortical neurons via Lentivirus- expressing GFP or GFP-NCL. The overexpression of GFP-NCL degraded the αSyn fibrils in whole cell lysates of the mouse primary cortical neurons (Fig. 6B). In addition, the levels of extracellular αSyn fibrils were slightly decreased by the transduction of GFP-NCL; however, this difference was not significant (Figs. 6C and 6D). These results were similar to those of the MEF experiments, thereby proving that the transduction of NCL promotes the clearance of αSyn even in neurons.

6. Transduction of NCL in the mouse SNpc ameliorates PD symptoms induced by αSyn fibrils

We also attempted to validate the degradation of αSyn by NCL transduction in a mouse model using a co-injection of Lenti-GFP or GFP-NCL with αSyn fibrils into the mouse SNpc. We observed that the transduction of GFP-NCL rescued the abnormal motor activity at 3- and 6-weeks post-injection (Fig. 7B). The level of tyrosine hydroxylase (TH) in the SNpc was slightly increased with the injection of GFP-NCL compared to GFP controls (Fig. 7C), but the phosphorylation of αSyn, a marker of αSyn aggregates,

showed a significant decrease in the SNpc of GFP-NCL models (Fig. 7D). However, the TH levels by the expression of GFP-NCL in the corpus striatum showed a slight decrease along with similar levels of αSyn phosphorylation (Supplementary Figs. 8A and 8B). Because the extracellular αSyn conformer is regarded as a source of neuroinflammation in the microglia (29, 30), we stained and counted the activated microglia in the SNpc and corpus striatum. The activated microglia were significantly decreased by the transduction of GFP-NCL in the SNpc (Fig. 7E) but not in the corpus striatum (Supplementary Fig. 8C). GFP or GFP-NCL expression was confirmed by western blot analysis of the midbrain lysate, and GFP-NCL slightly degraded high molecular weight (HWM)-αSyn via the induction of LC3B (Fig. 8A). To improve the ambiguous results of HWM- or Mono-αSyn levels along with GFP or GFP-NCL expression, we measured αSyn aggregates levels using ELISA. The levels of αSyn aggregates were significantly decreased by the transduction of GFP-NCL in the supernatants of crude extracts from the midbrain (Fig. 8B). Furthermore, the CTSD enzymatic activities in the midbrain lysate displayed higher levels in the GFP-NCL transduction relative to GFP controls (Fig. 8C). Based on these results, increasing NCL expression would be a feasible therapy for PD patients with related α-synucleinopathy via the degradation of αSyn aggregates.

Discussion

The distinct NCL disruption is dependent on the subcellular localization of αSyn. The accumulation of αSyn allows for neurons to become vulnerable (31). In most cases, αSyn accumulates in early/late endosomes or autophagosomes (32, 33). In addition, the decline in proteolytic activity due to the overload of cargo in autophagosomes and lysosomes is responsible for the accumulation of ROS and damaged mitochondria (34). Some reports have revealed that αSyn is also located and accumulated in the nuclei of dopaminergic neurons. In this case, nuclear accumulation of αSyn promotes the dysregulation of DNA repair or the cell cycle (24, 25). The cytotoxicity from the expression of NLS-αSyn showed a dramatic increase relative to WT-αSyn or NES-αSyn (Supplementary Fig. 1). The expression of NLS-αSyn formed the nucleolar morphology like beads on a string, which could expose the sites of ribosomal DNA (rDNA) transcription and processing, thereby enhancing ribosome assembly (Fig. 1B). These results may be due to increases in the molecules associated with neurotoxicity via disrupting the rendezvous of NCL on the nucleolar conformation with nuclear αSyn. It is possible that the increase in ribosome assembly via rDNA transcription induced by nuclear αSyn could upregulate protein synthesis, which initiates neuronal death. Contrary to a previous study that described the increase in neurotoxicity via the inhibition of histone acetylase by nuclear αSyn (35), our results were similar to another study where the inhibition of histone deacetylase induced apoptosis and cell cycle arrest (36). In an additional previous study, NCL interacted with DJ-1 and αSyn in the cytoplasm of MES cells, a dopaminergic cell line (23). This observation may explain why WT-αSyn and NES-αSyn displayed decreased endoNCL levels in the nuclei compared to Empty controls (Fig. 1B). Despite WT-αSyn interacting with NCL in the cytosol, WT-αSyn was occasionally located in the nucleus and showed significantly higher cytotoxicity than NES-αSyn. Given the aforementioned morphology of NLS-αSyn, a few WT-αSyn-expressing MEFs harbored an analogous nucleolar structure to cells transfected with NLS-αSyn (data not shown). The lower endoNCL levels in the nuclei of NES-αSyn-expressing MEFs resulted in the absence of nuclear αSyn compared to WT-αSyn due

to interactions between NCL and αSyn. The translocalization of NCL into the nuclei would be critical for their cellular function, and the interaction between NCL and αSyn could act as a nucleolar stressor. This nucleolar stress is also linked to oxidative stress (37), and the accumulation of αSyn is a culprit of oxidative stress (38). The inactivation of NCL accelerated cell cycle arrest via nucleolar stress (39). Treatment with arsenic disrupted the recruitment of NCL on the nucleoli (38), and H_2O_2-induced oxidative stress fragmented the nucleoli via the cleavage and downregulation of NCL (12). Thus, these results suggest that both the excess nuclear αSyn and interaction of NCL with αSyn could be responsible for PD progression via increasing neurotoxicity along with oxidative stress derived from the accumulation of αSyn.

The ectopic expression of NCL elevated the markers of the autophagy-lysosome pathway and clearance of accumulated αSyn via the increase in autophagosomes and active lysosomes (Fig. 3). In addition, the specific inhibitions of autophagy or lysosomal activity resulted in the abolishment of αSyn degradation by ectopic NCL expression, and inhibition of proteasomes by MG132 was not involved in NCL-mediated αSyn degradation (Fig. 4). These results support previous studies that described the autophagy-lysosome pathway as the predominant mechanism of degradation for accumulated αSyn (27, 40). NCL is also related to HSP70, which is known as a chaperone for αSyn degradation via chaperone-mediated autophagy (CMA) (41). The transduction of HSP70 rescued the degradation of NCL by H_2O_2-induced oxidative stress (15) and 1-methyl-4-phenyl-1,2,3,6-tetrahydropyridine (MPTP)-mediated dopaminergic degeneration in the mouse model (42). The inductions of NCL and HSP70 were essential for the regeneration of hepatocytes (43), implying that the coordination between HSP70 and NCL is important for the recovery of dopaminergic neurons. In addition to these results suggesting that the induction of NCL levels may be a therapeutic target for PD, our study elucidated the positive effects of NCL on αSyn degradation for the first time. However, the suppression of cell surface-expressed NCL using aptamers and antagonists is a novel drug target for cancer (13, 44). Thus, we tested the levels of the epidermal growth factor receptor (EGFR), also known as a neuroblastoma marker (45), in the midbrain. The transduction of GFP-NCL showed no significant difference in EGFR levels compared to GFP transduction (Supplementary Fig. 9), so the elevation of NCL in the SNpc does not appear to promote carcinogenesis.

The enhancement of αSyn degradation has been considered as a major drug target for PD. In this report, we demonstrated that NCL transduction would a feasible therapeutic method for the clearance of αSyn aggregates in the mouse model (Figs. 7 and 8). A hexanucleotide repeat expansion in *C9orf72* (*C9orf72*-HRE), a culprit of amyotrophic lateral sclerosis (ALS), interacted with NCL to disrupt the nuclear localization of NCL in *C9orf72*-HRE in ALS patients' cells, thereby aggravating nucleolar stress-induced neuronal death (46, 47). These results support that the drugs maintaining or recovering both the levels and functions of NCL would be crucial for the discovery of potential therapeutic targets for neurodegenerative diseases.

Conclusions

Upregulating NCL levels and functions may be an appropriate drug target for PD therapy via facilitating the clearance of αSyn in the SNpc. This research could be a driving force for and asset to future studies as well as the discovery of a novel drug that increases NCL levels to treat PD.

Abbreviations

αSyn
Alpha-synuclein
PD
Parkinson’s disease
NCL
Nucleolin
MEF
Mouse embryonic fibroblasts
GFP
Green fluorescent protein
SNpc
Substantia nigra pars compacta
LB
Lewy body
LN
Lewy neurite
HSP70
Heat shock protein 70
ROS
Reactive oxygen species
DMEM
Dulbecco's Modified Eagle Medium
FBS
Fetal bovine serum
PS
Penicillin/streptomycin
PBS
Phosphate-buffered saline
PCR
Polymerase chain reaction
ELISA
Enzyme-linked immunosorbent assay
endoNCL
Endogenous NCL

NLS
Nuclear localization signal
NES
nuclear escape signal
Flag-αSyn
Flag-tagged αSyn
WT-αSyn
Wild type Flag-αSyn
NES-αSyn
Flag-αSyn with NES
NLS-αSyn
Flag-αSyn with NLS
Tx-100 sol
TritonX-100 soluble
Tx-100 insol
TritonX-100 insoluble
Flag-p21
Flag-tagged p21
LC3B
Light Chain 3B
LAMP1
lysosome-associate membrane protein 1
CTSD
cathepsin D
3-MA
3-Methyladenine
Baf A1
Bailomycin A1
HMW
High molecular weight
CMA
Chaperone-mediated autophagy
MPTP
yl-4-phenyl-1,2,3,6-tetrahydropyridine
EGFR
epidermal growth factor receptor
ALS
amyotrophic lateral sclerosis

Declarations

Ethics approval

All care processes were conducted in accordance with the provisions of the Dankook Animal Ethics Committee (Dankook IACUC, 18-026).

Competing interest

The authors declare no competing interest.

Data availability

The datasets generated during and/or analyzed during the current study are available from the corresponding author on reasonable request.

Author Contributions

DH designed all experiments in this study and wrote this manuscript. Most of experimental results were performed and analyzed by DH, DN and SJ. MS and SP isolated and cultured a rat primary cortical neuron. WS and IS advised the experimental approaches and writing. All authors read and approved the final manuscript.

Funding

This work was supported by grants from the Basic Science Research Program (NRF-2017R1D1A1B03033814 to DH) in Republic of Korea.

Acknowledgments

We appreciated to NeuroVis for the service of animal experiments. And we would like to thank Editage (www.editage.co.kr) for English language editing.

References

1. Calne DB, Mizuno Y. The neuromythology of Parkinson's Disease. Parkinsonism Relat Disord. 2004;10(5):319–22.
2. Stefanis L. α-Synuclein in Parkinson's disease. Cold Spring Harb Perspect Med. 2012;2(2):a009399-a.
3. Webb JL, Ravikumar B, Atkins J, Skepper JN, Rubinsztein DC. Alpha-Synuclein is degraded by both autophagy and the proteasome. J Biol Chem. 2003;278(27):25009–13.
4. Roberts HL, Brown DR. Seeking a mechanism for the toxicity of oligomeric α-synuclein. Biomolecules. 2015;5(2):282–305.
5. Sato S, Uchihara T, Fukuda T, Noda S, Kondo H, Saiki S, et al. Loss of autophagy in dopaminergic neurons causes Lewy pathology and motor dysfunction in aged mice. Sci Rep. 2018;8(1):2813.

6. Chen Q-Q, Haikal C, Li W, Li M-T, Wang Z-Y, Li J-Y. Age-dependent alpha-synuclein accumulation and aggregation in the colon of a transgenic mouse model of Parkinson's disease. Transl Neurodegener. 2018;7:13-.
7. Hijaz BA, Volpicelli-Daley LA. Initiation and propagation of α-synuclein aggregation in the nervous system. Molecular Neurodegeneration. 2020;15(1):19.
8. Kurnik M, Sahin C, Andersen CB, Lorenzen N, Giehm L, Mohammad-Beigi H, et al. Potent α-Synuclein Aggregation Inhibitors, Identified by High-Throughput Screening, Mainly Target the Monomeric State. Cell Chemical Biology. 2018;25(11):1389 – 402.e9.
9. Pujols J, Peña-Díaz S, Lázaro DF, Peccati F, Pinheiro F, González D, et al. Small molecule inhibits α-synuclein aggregation, disrupts amyloid fibrils, and prevents degeneration of dopaminergic neurons. Proceedings of the National Academy of Sciences. 2018;115(41):10481-6.
10. Ma N, Matsunaga S, Takata H, Ono-Maniwa R, Uchiyama S, Fukui K. Nucleolin functions in nucleolus formation and chromosome congression. J Cell Sci. 2007;120(12):2091–105.
11. Kobayashi J, Fujimoto H, Sato J, Hayashi I, Burma S, Matsuura S, et al. Nucleolin participates in DNA double-strand break-induced damage response through MDC1-dependent pathway. PLoS One. 2012;7(11):e49245-e.
12. Zhang B, Wang H, Jiang B, Liang P, Liu M, Deng G, et al. Nucleolin/C23 is a negative regulator of hydrogen peroxide-induced apoptosis in HUVECs. Cell Stress Chaperones. 2010;15(3):249–57.
13. Benedetti E, Antonosante A, d'Angelo M, Cristiano L, Galzio R, Destouches D, et al. Nucleolin antagonist triggers autophagic cell death in human glioblastoma primary cells and decreased in vivo tumor growth in orthotopic brain tumor model. Oncotarget. 2015;6(39):42091–104.
14. Goldstein M, Derheimer FA, Tait-Mulder J, Kastan MB. Nucleolin mediates nucleosome disruption critical for DNA double-strand break repair. Proc Natl Acad Sci U S A. 2013;110(42):16874–9.
15. Jiang B, Zhang B, Liang P, Song J, Deng H, Tu Z, et al. Nucleolin/C23 mediates the antiapoptotic effect of heat shock protein 70 during oxidative stress. Febs j. 2010;277(3):642–52.
16. Caudle WM, Kitsou E, Li J, Bradner J, Zhang J. A role for a novel protein, nucleolin, in Parkinson's disease. Neurosci Lett. 2009;459(1):11–5.
17. Scudamore O, Ciossek T. Increased Oxidative Stress Exacerbates α-Synuclein Aggregation In Vivo. J Neuropathol Exp Neurol. 2018;77(6):443–53.
18. Ho DH, Kim H, Kim J, Sim H, Ahn H, Kim J, et al. Leucine-Rich Repeat Kinase 2 (LRRK2) phosphorylates p53 and induces p21(WAF1/CIP1) expression. Mol Brain. 2015;8:54.
19. Ho DH, Seol W, Son I. Upregulation of the p53-p21 pathway by G2019S LRRK2 contributes to the cellular senescence and accumulation of α-synuclein. Cell Cycle. 2019;18(4):467–75.
20. Daleum Nam J-YL, Lee M, Kim J, Seol W, Ilhong Son and Dong Hwan Ho. Detection and Assessment of α-Synuclein Oligomers in the Urine of Parkinson's Disease Patients. Journal of Parkinson's Disease. 2020:In press.

21. Seo MK, McIntyre RS, Cho HY, Lee CH, Park SW, Mansur RB, et al. Tianeptine induces mTORC1 activation in rat hippocampal neurons under toxic conditions. Psychopharmacology. 2016;233(13):2617–27.
22. Maskey D, Pradhan J, Aryal B, Lee CM, Choi IY, Park KS, et al. Chronic 835-MHz radiofrequency exposure to mice hippocampus alters the distribution of calbindin and GFAP immunoreactivity. Brain Res. 2010;1346:237–46.
23. Jin J, Li GJ, Davis J, Zhu D, Wang Y, Pan C, et al. Identification of novel proteins associated with both alpha-synuclein and DJ-1. Molecular cellular proteomics: MCP. 2007;6(5):845–59.
24. Pinho R, Paiva I, Jercic KG, Fonseca-Ornelas L, Gerhardt E, Fahlbusch C, et al. Nuclear localization and phosphorylation modulate pathological effects of alpha-synuclein. Hum Mol Genet. 2019;28(1):31–50.
25. Ma KL, Song LK, Yuan YH, Zhang Y, Han N, Gao K, et al. The nuclear accumulation of alpha-synuclein is mediated by importin alpha and promotes neurotoxicity by accelerating the cell cycle. Neuropharmacology. 2014;82:132–42.
26. Koch JC, Bitow F, Haack J, d'Hedouville Z, Zhang JN, Tönges L, et al. Alpha-Synuclein affects neurite morphology, autophagy, vesicle transport and axonal degeneration in CNS neurons. Cell Death Dis. 2015;6(7):e1811-e.
27. Ebrahimi-Fakhari D, Cantuti-Castelvetri I, Fan Z, Rockenstein E, Masliah E, Hyman BT, et al. Distinct roles in vivo for the ubiquitin-proteasome system and the autophagy-lysosomal pathway in the degradation of α-synuclein. J Neurosci. 2011;31(41):14508–20.
28. Singh SK, Dutta A, Modi G. α-Synuclein aggregation modulation: an emerging approach for the treatment of Parkinson's disease. Future Med Chem. 2017;9(10):1039–53.
29. Zhang W, Wang T, Pei Z, Miller DS, Wu X, Block ML, et al. Aggregated α-synuclein activates microglia: a process leading to disease progression in Parkinson’s disease. FASEB J. 2005;19(6):533–42.
30. Kim C, Ho DH, Suk JE, You S, Michael S, Kang J, et al. Neuron-released oligomeric α-synuclein is an endogenous agonist of TLR2 for paracrine activation of microglia. Nat Commun. 2013;4:1562.
31. Surmeier DJ, Obeso JA, Halliday GM. Selective neuronal vulnerability in Parkinson disease. Nat Rev Neurosci. 2017;18(2):101–13.
32. Kett LR, Dauer WT. Endolysosomal dysfunction in Parkinson's disease: Recent developments and future challenges. Mov Disord. 2016;31(10):1433–43.
33. Arotcarena M-L, Teil M, Dehay B. Autophagy in Synucleinopathy: The Overwhelmed and Defective Machinery. Cells. 2019;8(6):565.
34. Festa BP, Chen Z, Berquez M, Debaix H, Tokonami N, Prange JA, et al. Impaired autophagy bridges lysosomal storage disease and epithelial dysfunction in the kidney. Nat Commun. 2018;9(1):161.
35. Kontopoulos E, Parvin JD, Feany MB. α-synuclein acts in the nucleus to inhibit histone acetylation and promote neurotoxicity. Hum Mol Genet. 2006;15(20):3012–23.

36. Bao L, Diao H, Dong N, Su X, Wang B, Mo Q, et al. Histone deacetylase inhibitor induces cell apoptosis and cycle arrest in lung cancer cells via mitochondrial injury and p53 up-acetylation. Cell Biol Toxicol. 2016;32(6):469–82.
37. Lewinska A, Wnuk M, Grzelak A, Bartosz G. Nucleolus as an oxidative stress sensor in the yeast Saccharomyces cerevisiae. Redox Rep. 2010;15(2):87–96.
38. Musgrove RE, Helwig M, Bae E-J, Aboutalebi H, Lee S-J, Ulusoy A, et al. Oxidative stress in vagal neurons promotes parkinsonian pathology and intercellular α-synuclein transfer. J Clin Invest. 2019;130(9):3738–53.
39. Ugrinova I, Monier K, Ivaldi C, Thiry M, Storck S, Mongelard F, et al. Inactivation of nucleolin leads to nucleolar disruption, cell cycle arrest and defects in centrosome duplication. BMC Mol Biol. 2007;8:66.
40. Lee HJ, Khoshaghideh F, Patel S, Lee SJ. Clearance of alpha-synuclein oligomeric intermediates via the lysosomal degradation pathway. J Neurosci. 2004;24(8):1888–96.
41. Cuervo AM, Stefanis L, Fredenburg R, Lansbury PT, Sulzer D. Impaired degradation of mutant alpha-synuclein by chaperone-mediated autophagy. Science. 2004;305(5688):1292–5.
42. Dong Z, Wolfer DP, Lipp HP, Büeler H. Hsp70 gene transfer by adeno-associated virus inhibits MPTP-induced nigrostriatal degeneration in the mouse model of Parkinson disease. Mol Ther. 2005;11(1):80–8.
43. Konishi T, Karasaki Y, Nomoto M, Ohmori H, Shibata K, Abe T, et al. Induction of heat shock protein 70 and nucleolin and their intracellular distribution during early stage of liver regeneration. J Biochem. 1995;117(6):1170–7.
44. Mosafer J, Mokhtarzadeh A. Cell Surface Nucleolin as a Promising Receptor for Effective AS1411 Aptamer-Mediated Targeted Drug Delivery into Cancer Cells. Curr Drug Deliv. 2018;15(9):1323–9.
45. Zheng C, Shen R, Li K, Zheng N, Zong Y, Ye D, et al. Epidermal growth factor receptor is overexpressed in neuroblastoma tissues and cells. Acta Biochim Biophys Sin (Shanghai). 2016;48(8):762–7.
46. Haeusler AR, Donnelly CJ, Periz G, Simko EA, Shaw PG, Kim MS, et al. C9orf72 nucleotide repeat structures initiate molecular cascades of disease. Nature. 2014;507(7491):195–200.
47. O'Rourke JG, Bogdanik L, Muhammad AK, Gendron TF, Kim KJ, Austin A, et al. C9orf72 BAC Transgenic Mice Display Typical Pathologic Features of ALS/FTD. Neuron. 2015;88(5):892–901.

Figures

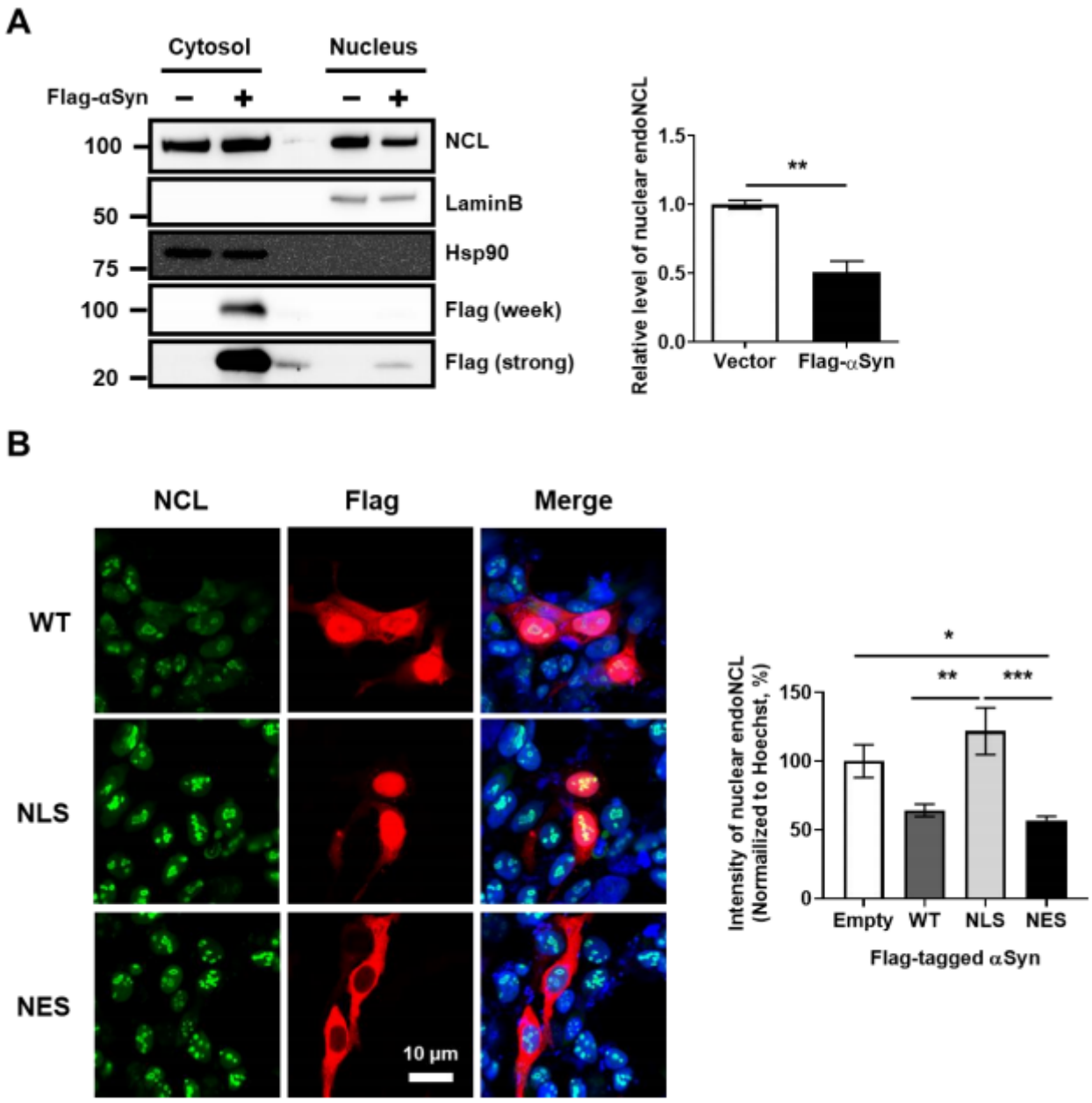

Figure 1

Expression of αSyn changes the nuclear NCL. (A) The levels of nuclear NCL were analyzed using cytosol/nuclear fractionation of MEFs transfected by Flag-αSyn for 24 h. Student's t-test; **p < 0.001; n=3. (B) The NCL structure localized in the nuclei of the MEFs was altered by WT (WT-αSyn), NLS (NLS-αSyn), or NES (NES-αSyn). One-way ANOVA (analysis of variance) with Bonferroni's post-hoc test; *p < 0.05, **p < 0.01, ***p < 0.001; n=3 (cells for Empty=26, WT=23, NLS=28, and NES=28). Data are represented as mean ± SEM.

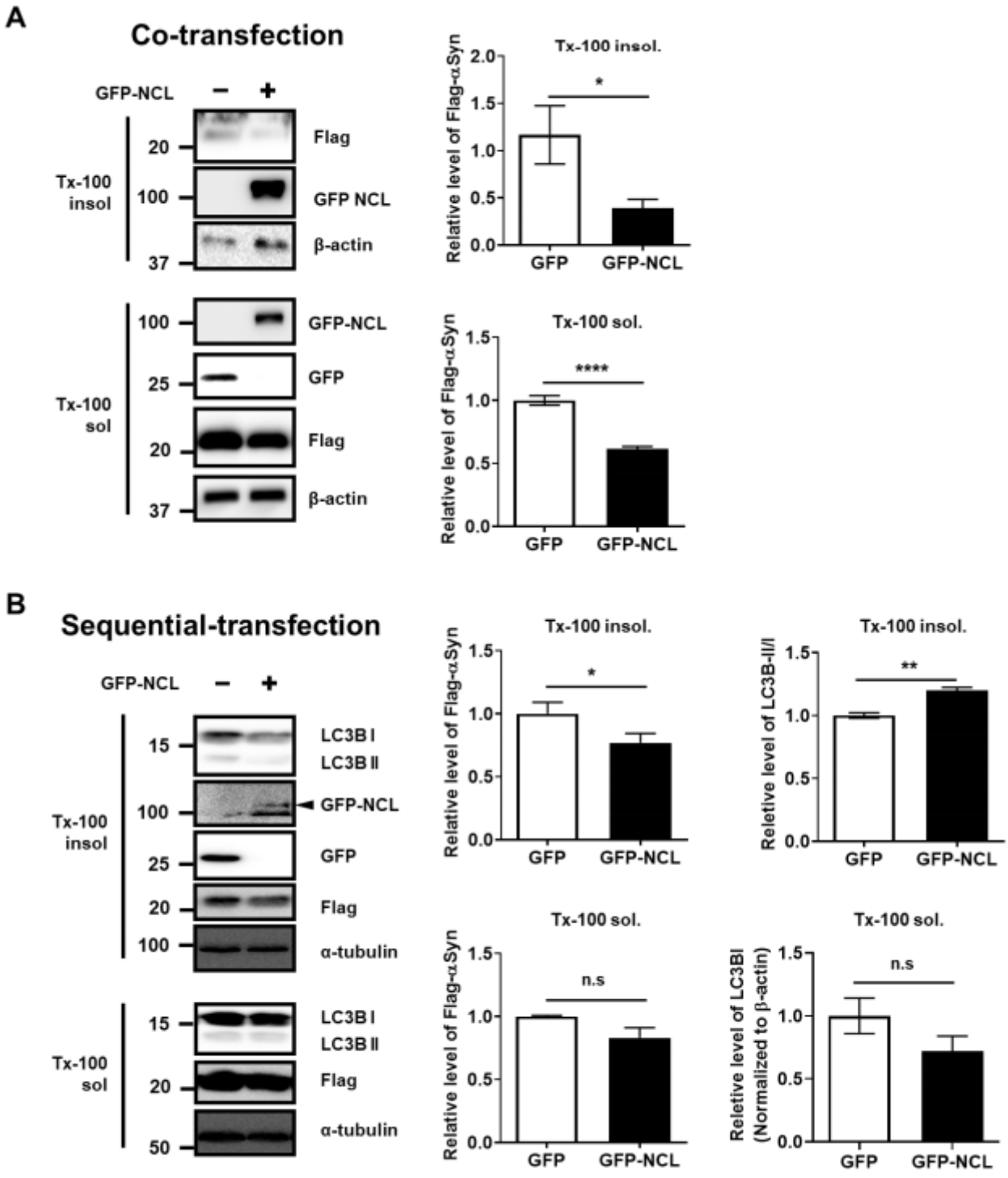

Figure 2

Expression of NCL decreases αSyn overexpression. (A) Flag-αSyn and GFP/GFP-NCL were co-transfected for 24 h in MEFs. Student's t-test, *p < 0.05, ****p < 0.0001; n=6. (B) GFP/GFP-NCL were transfected for 24 h following the transfection of Flag-αSyn for 12 h in MEFs. Student's t-test, *p < 0.05, **p < 0.01; n.s: not significant; n=3. Data are represented as mean ± SEM.

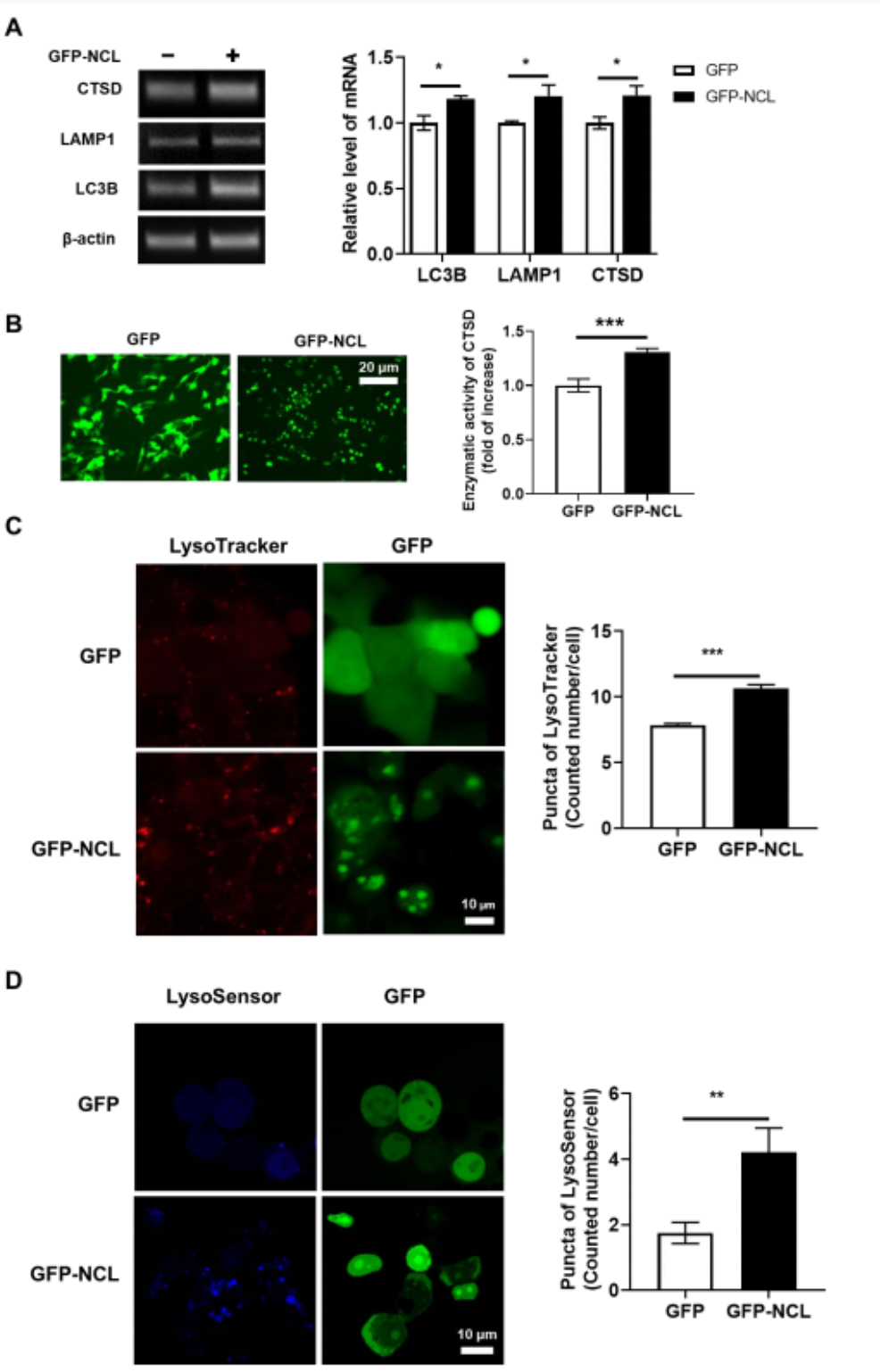

Figure 3

Elevation of autophagy-lysosomal degradation by the expression of NCL. (A) The levels of mRNA expression were analyzed in MEFs transfected with GFP/GFP-NCL for 24 h; n=6. (B) The activity of the lysosomal enzyme CTSD was measured in MEFs transfected with GFP/GFP-NCL for 24 h; n=9. (C) MEFs were treated with LysoTracker Red DND-99 (75 nM) for 2 h following transfection with GFP/GFP-NCL for 24 h before the cells were fixed and analyzed; n=3 (cells with GFP=55 and GFP-NCL=56). (D) The

lysosomes with acidic conditions in MEFs transfected with GFP/GFP-NCL for 24 h were detected using LysoSensor Blue DND-167 (1 μM) before images of the cells were captured live following a brief PBS washing. Student's t-test, *p < 0.05, **p < 0.01, ***p < 0.001; n=4 (cells of GFP=227, GFP-NCL=164). Data are represented as mean ± SEM.

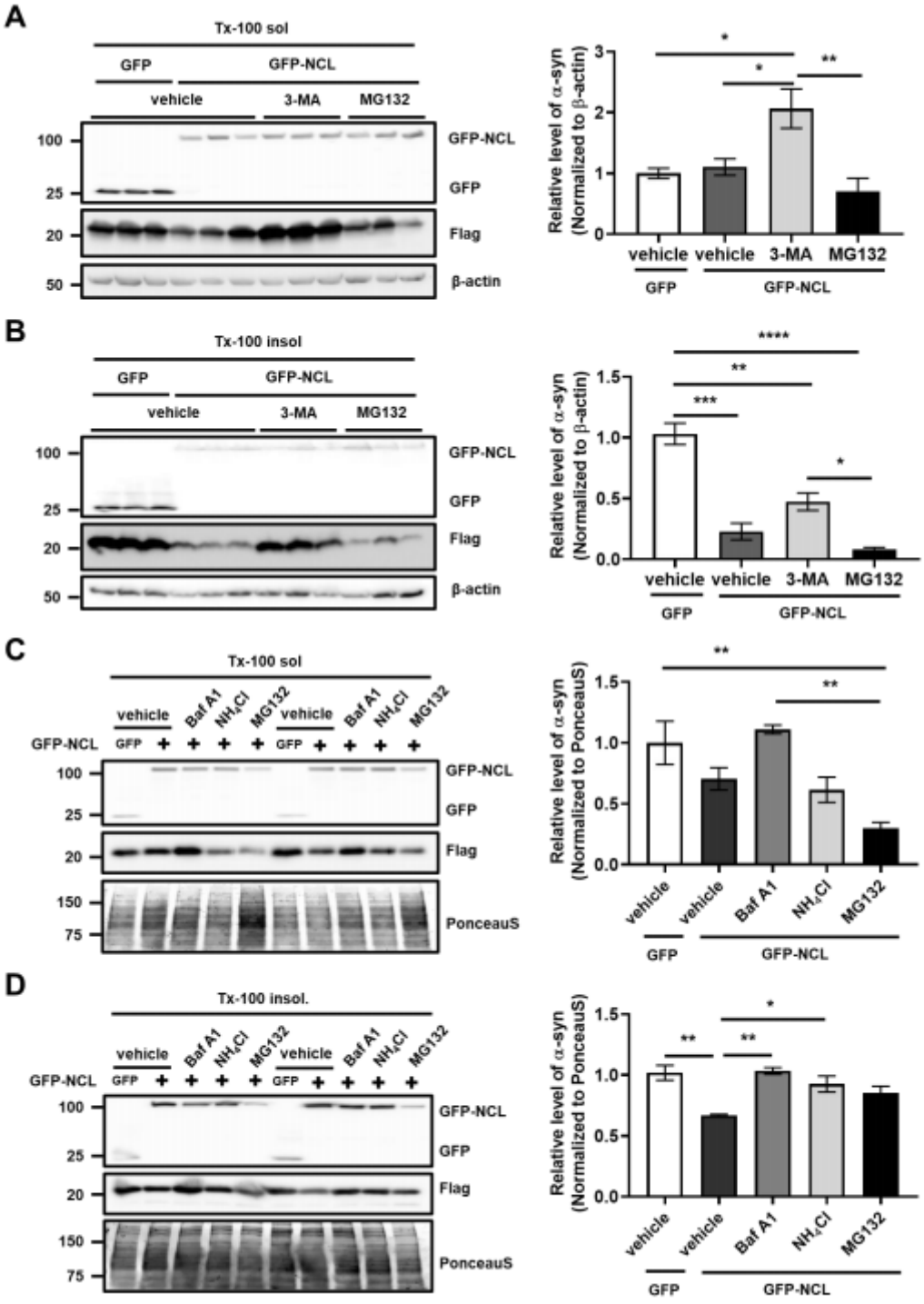

Figure 4

Inhibition of autophagy-lysosomal degradation devastates the effect of NCL expression. (A-B) MEFs transfected with GFP or GFP-NCL for 24 h following 12 h transfection of Flag-αSyn were treated with 1

mM 3-MA, 2.5 μM MG132, or DMSO (vehicle) for 6 h. (C-D) After the sequential transfection of GFP/GFP-NCL for 24 h following the transfection of Flag-αSyn for 12 h in MEFs, 0.5 μM Baf A1, 5 mM NH4Cl, 2.5 μM MG132, or DMSO (vehicle) was added for 6 h. One-way ANOVA with Bonferroni's post-hoc test, *p < 0.05, **p < 0.01, ***p < 0.001, ****p < 0.0001; n=3. Data are represented as mean ± SEM.

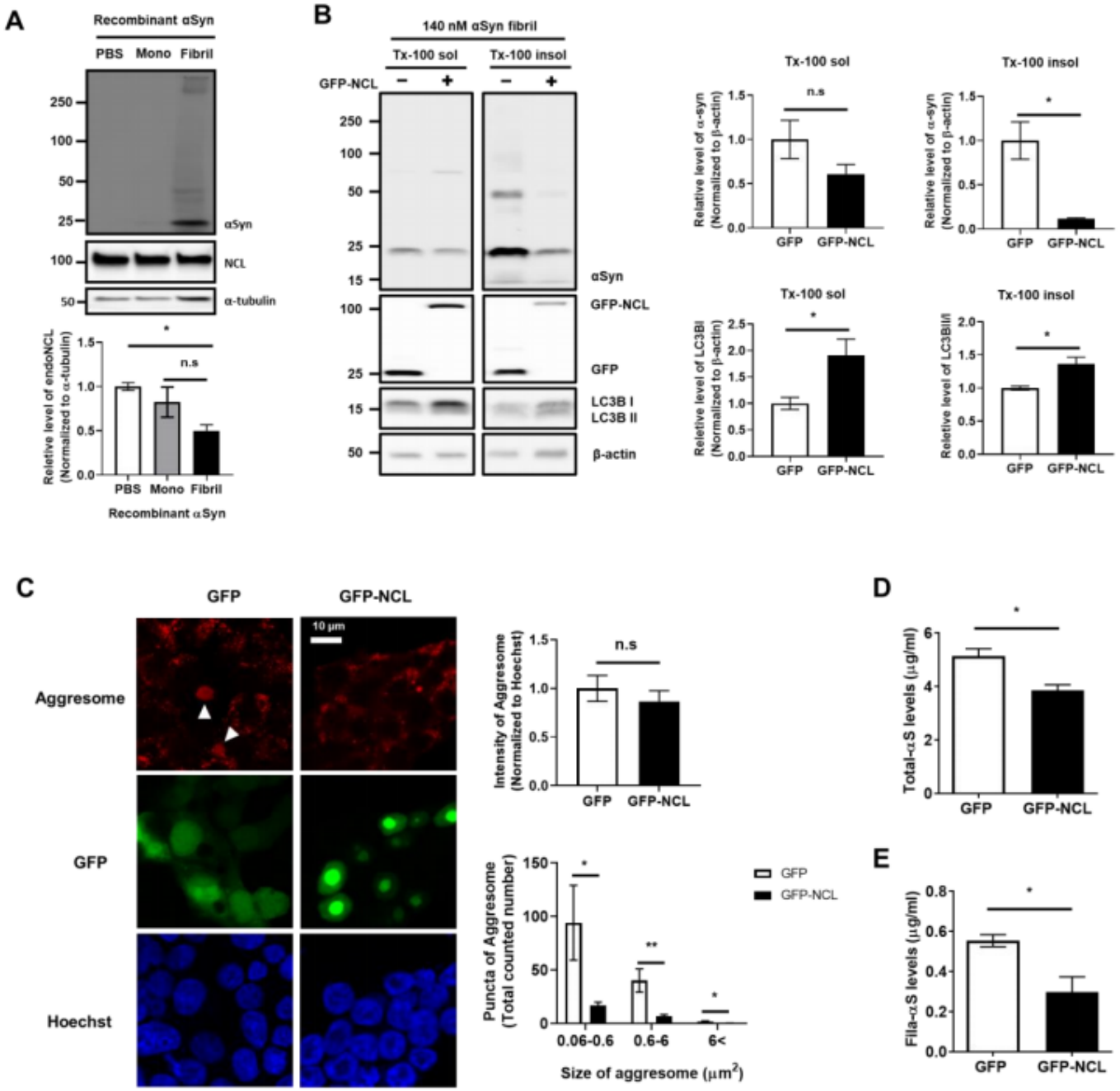

Figure 5

Clearance of extracellular αSyn aggregates by the expression of NCL. (A) PBS as a control, 700 nM monomer (Mono), or fibril (Fibril)-recombinant αSyn were treated for 24 h. (B) αSyn fibrils (700 nM) were pre-treated for 6 h before MEFs were transfected with GFP or GFP-NCL for 24 h. (C) The GFP/GFP-NCL-transfected MEFs were fixed and stained with a Proteostat Aggresome Detection Kit. The number and size of red Aggresome puncta in the GFP/GFP-NCL-positive cells were analyzed by ImageJ (cells with

GFP=78, GFP-NCL=36. (D) The amount of total αSyn [Total-αS] and (E) filament-like αSyn [Fila-αS] in culture media from (C) were analyzed established ELISA. Student's t-test, *; p<0.05, **; p<0.01, n.s; not significant, n=4. Data are represented as mean ± SEM.

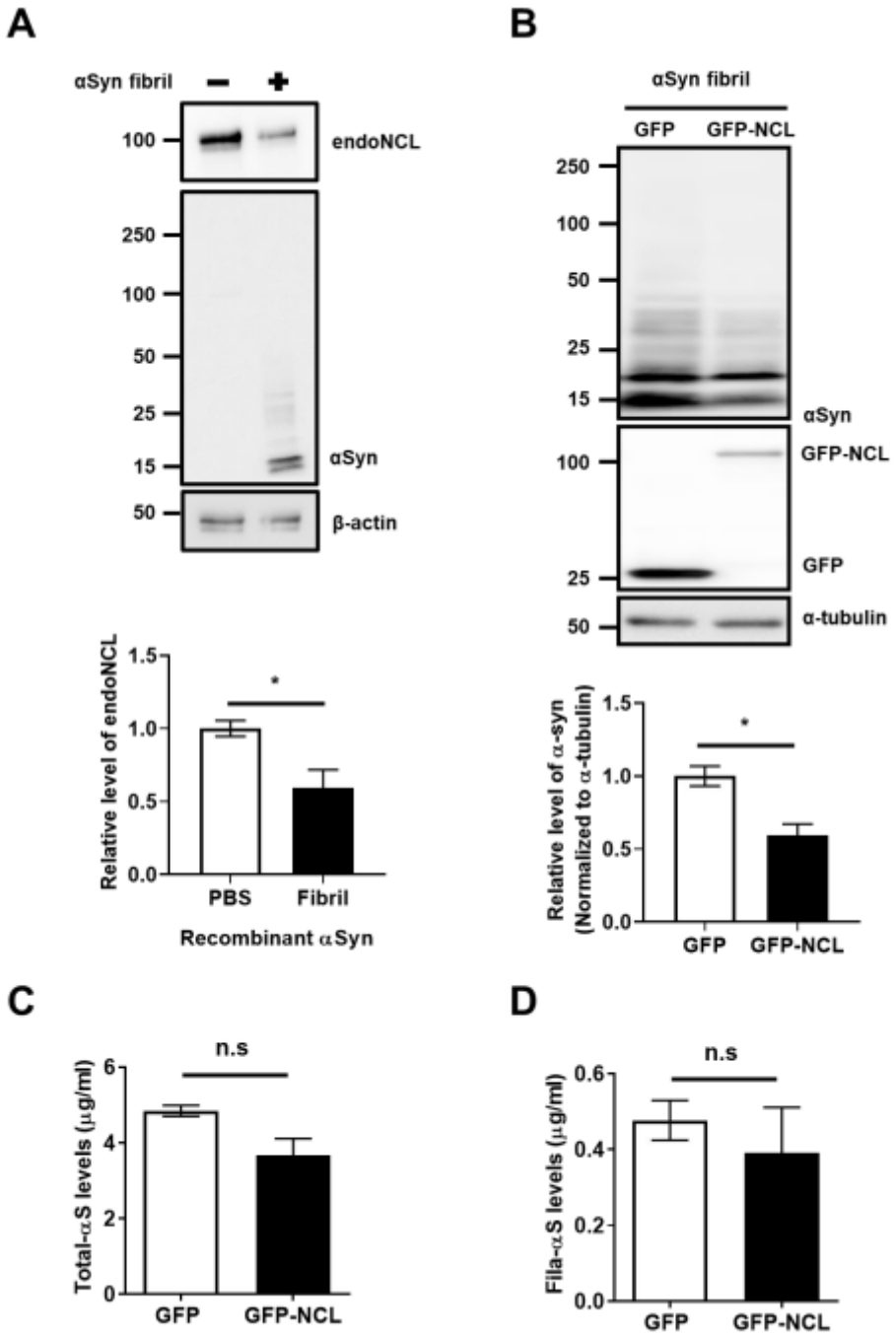

Figure 6

Expression of NCL in neuron promote the degradation of extracellular αSyn fibril. (A) αSyn fibril (700 nM) were treated for 24 h in rat primary cortical neuron. (B) Lenti viral infection of GFP/GFP-NCL were performed for 24h following the pre-treatment of 700 nM αSyn fibril for 6 h. The culture media of (B) were

collected and analyzed by the ELISA for Total-αS (C) or Fila-αS (D). Data are represented as mean ± SEM. Student's t-test, *; p<0.05, n.s; not significant, n=4.

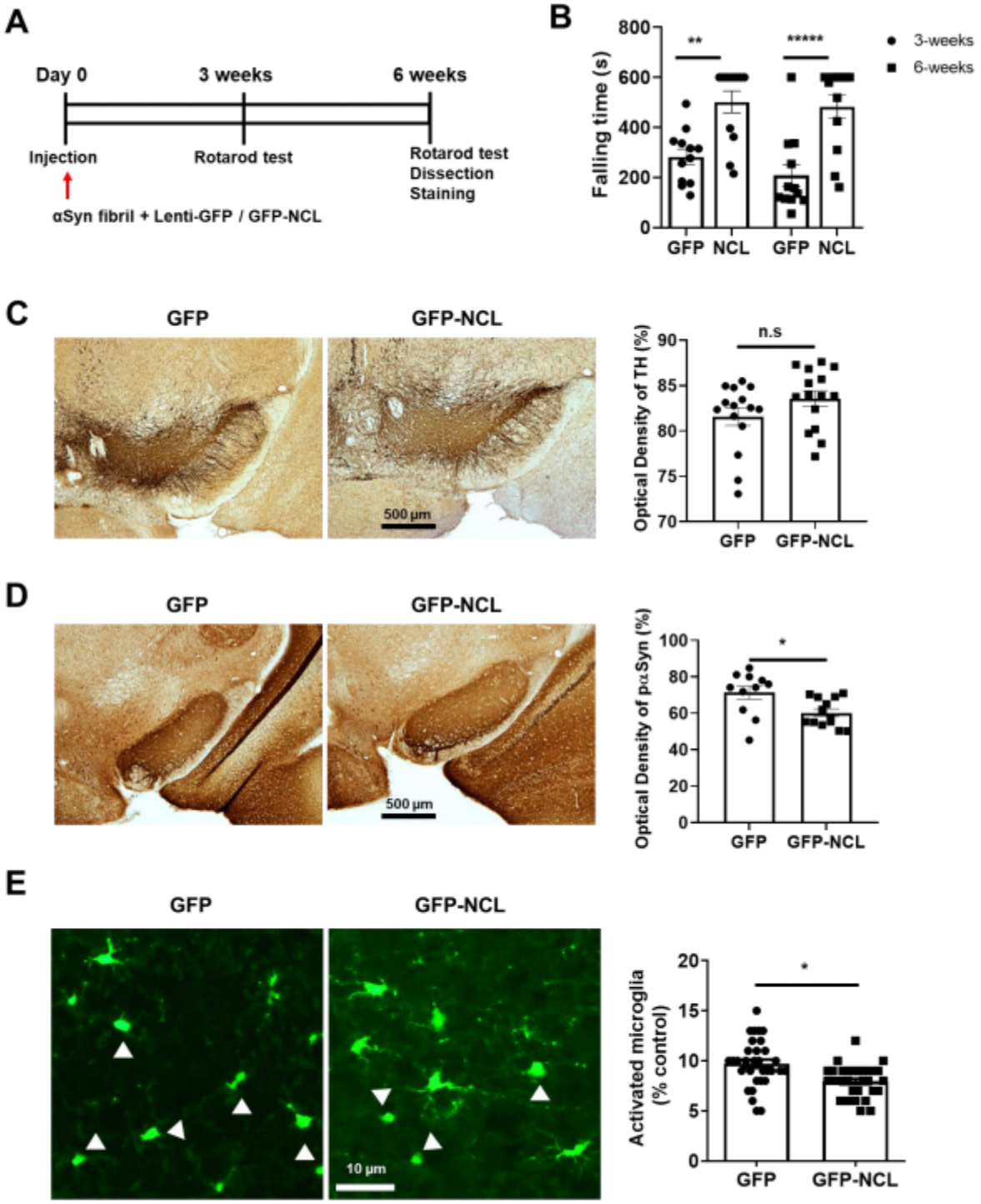

Figure 7

Expression of transduced NCL in mouse SNpc rescue α-synucleinopathy. (A) The scheme of mouse experiment. (B) Mice injected with lenti-viral GFP/GFP-NCL and αSyn fibril in SNpc for indicated times were examined with the rotarod test. (C) TH or (D) phosphorylation on S129 of αSyn (pαSyn) was used

for a marker of DA neuron or aggregates of αSyn. (E) Iba1 was used for a marker of microglia, and the microglia, which showed the shortening of their processes, was counted as an active microglia (arrowheads). Data are represented as mean ± SEM. Student's t-test, *; p<0.05, **; p<0.01, ****; p<0.0001, n=4 [slices for GFP=15 (A), 11 (B), 23 (C), GFP-NCL=15 (A), 13 (B), 32 (C)].

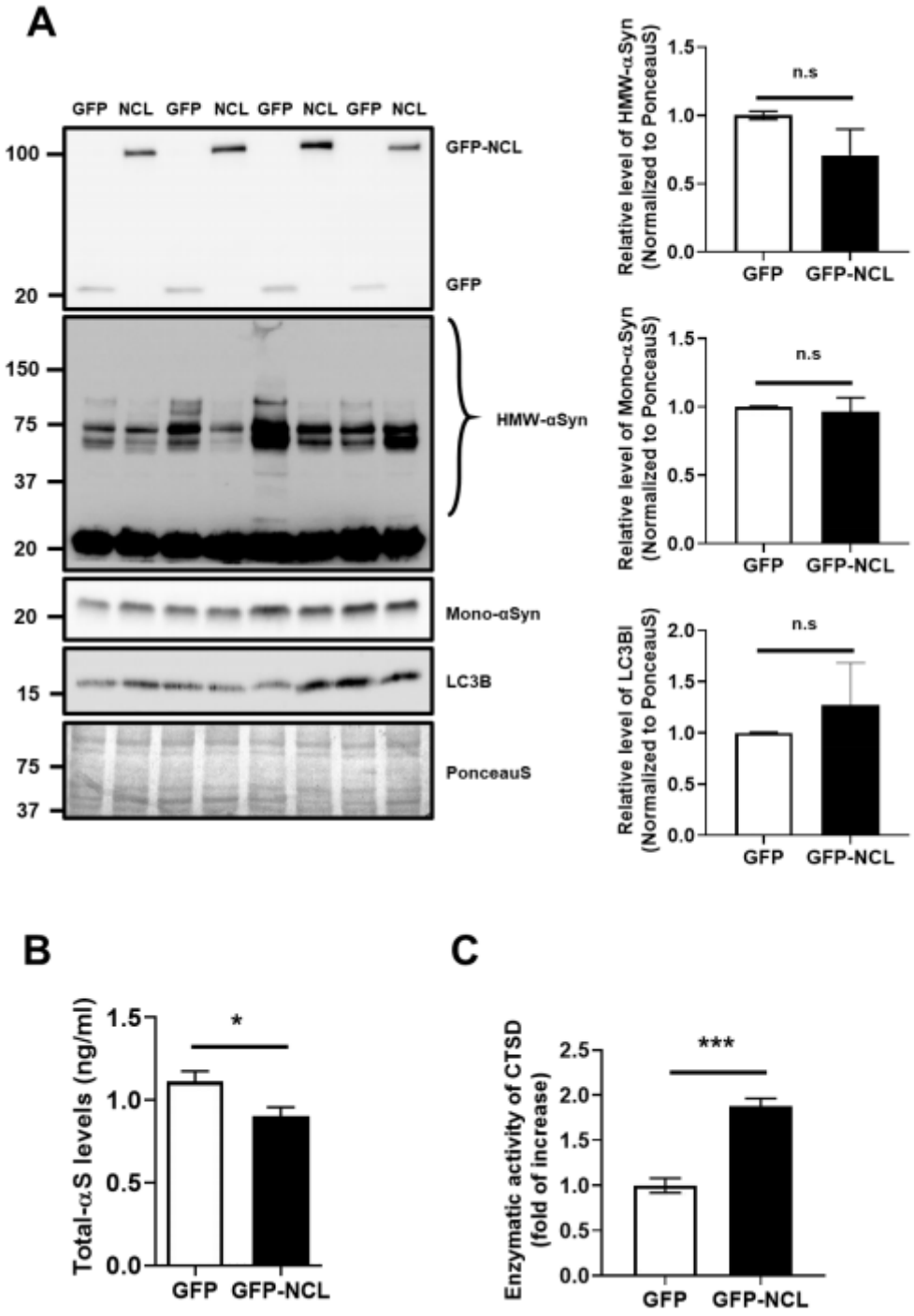

Figure 8

Rescued α-synucleinopathy in mouse SNpc by the expression NCL is mediated by the autophagy-lysosomal degradation. (A) The midbrain lysates from mice introduced with lenti-viral GFP/GFP-NCL and

αSyn fibril was analyzed by Western blot. (B) The levels of whole αSyn in midbrain lysate was analyzed Total-αS ELISA. (C) The lysates from midbrain was subjected to CTSD activity assay to represent the activity of lysosomal enzymes. Data are represented as mean ± SEM. Student's t-test, *; $p<0.05$, ***; $p<0.001$, n=4.

Supplementary Files

This is a list of supplementary files associated with this preprint. Click to download.

- SF.pdf